IOPscience iopscience.iop.org

Home Search Collections Journals About Contact us My IOPscience

Generalized regressive motion: a visual cue to collision

This content has been downloaded from IOPscience. Please scroll down to see the full text.

2016 Bioinspir. Biomim. 11 046008

(http://iopscience.iop.org/1748-3190/11/4/046008)

View the table of contents for this issue, or go to the journal homepage for more

Download details:

IP Address: 131.215.70.231
This content was downloaded on 30/09/2016 at 16:07

Please note that terms and conditions apply.

You may also be interested in:

A novel distributed swarm control strategy based on coupled signal oscillators
Manfred Hartbauer and Heiner Römer

RoboFish: increased acceptance of interactive robotic fish with realistic eyes and natural motion patterns by live Trinidadian guppies
Tim Landgraf, David Bierbach, Hai Nguyen et al.

Locomotion of Mexican jumping beans
Daniel M West, Ishan K Lal, Michael J Leamy et al.

Controlling legs for locomotion—insights from robotics and neurobiology
Thomas Buschmann, Alexander Ewald, Arndt von Twickel et al.

Monocular distance estimation from optic flow during active landing maneuvers
Floris van Breugel, Kristi Morgansen and Michael H Dickinson

Flocking algorithm for autonomous flying robots
Csaba Virágh, Gábor Vásárhelyi, Norbert Tarcai et al.

A biomimetic vision-based hovercraft accounts for bees' complex behaviour in various corridors
Frédéric L Roubieu, Julien R Serres, Fabien Colonnier et al.

IOP Publishing Bioinspir. Biomim. 11 (2016) 046008 doi:10.1088/1748-3190/11/4/046008

Bioinspiration & Biomimetics

OPEN ACCESS

RECEIVED
17 November 2015

REVISED
19 May 2016

ACCEPTED FOR PUBLICATION
7 June 2016

PUBLISHED
18 July 2016

Original content from this work may be used under the terms of the Creative Commons Attribution 3.0 licence.

Any further distribution of this work must maintain attribution to the author(s) and the title of the work, journal citation and DOI.

PAPER

Generalized regressive motion: a visual cue to collision

Krzysztof Chalupka[1], **Michael Dickinson**[2] **and Pietro Perona**[3]

[1] Computation and Neural Systems California Insistute of Technology, USA
[2] Biology California Institute of Technology, USA
[3] Electrical Engineering California Institute of Technology, USA

E-mail: kjchalup@caltech.edu

Keywords: locomotion, optic flow, drosophila, low-power vision, looming, agent-based modeling

Supplementary material for this article is available online

Abstract

Brains and sensory systems evolved to guide motion. Central to this task is controlling the approach to stationary obstacles and detecting moving organisms. Looming has been proposed as the main monocular visual cue for detecting the approach of other animals and avoiding collisions with stationary obstacles. Elegant neural mechanisms for looming detection have been found in the brain of insects and vertebrates. However, looming has not been analyzed in the context of collisions between two moving animals. We propose an alternative strategy, generalized regressive motion (GRM), which is consistent with recently observed behavior in fruit flies. Geometric analysis proves that GRM is a reliable cue to collision among conspecifics, whereas agent-based modeling suggests that GRM is a better cue than looming as a means to detect approach, prevent collisions and maintain mobility.

Introduction

Animals move to forage, approach potential mates, chase prey, escape from predators, and to maintain their position within a group. They must do so in environments that are often cluttered by rocks, plants and other moving animals. Whether the goal is making or avoiding contact, it is valuable to detect the proximity of both stationary and moving entities.

Looming, defined by Gibson as a visual pattern expanding symmetrically on the retina (Schiff *et al* 1962), is commonly believed to be a robust and reliable monocular visual cue to impending collision[4]. It is often understood as a loosely-defined group of visual stimuli rather than a specific mechanism, with an underlying idea that an object approaching with a constant velocity produces expanding patterns on the observer's retina. When an animal is stationary, looming is a sufficient cue to detect approaching objects. When a moving animal is on a collision course with a stationary obstacle, time-to-collision can be estimated from looming patterns even when distance is unknown (Lee and Reddish 1981, Wang and Frost 1992). It is generally accepted that looming is a cue used by various animals to avoid stationary obstacles, and elegant neural mechanisms for its detection have been unveiled. Experiments have revealed looming-sensitive neural pathways in many animals. The DCMD/LGMD neurons of the locust (Rind and Simmons 1992, Hatsopoulos *et al* 1995, Gabbiani *et al* 2002) as well as the pigeon nucleus rotundus (Sun and Frost 1998) and the goldfish Mauthner cell (Preuss *et al* 2006) respond to divergence of image edges. Finally, the fruit fly uses looming-sensitive neurons during navigation (Fotowat and Fayyazuddin (2009), de Vries and Clandinin (2012); see also discussion).

Looming has been analyzed in the setting where either the animal or the obstacle is stationary. This is in contrast to regressive motion, used by the fruit fly to avoid collisions among multiple moving animals (Zabala *et al* 2012). Neural mechanisms behind regressive motion-driven behavior are unknown (Zabala *et al* 2012), but correlational motion detectors likely used by the fruit fly (Eichner *et al* 2011, Takemura *et al* 2013) can form a solid basis for regressive motion detection. The ecological usefulness of regressive

[4] We will call 'collision' an event in which one moving agent comes into physical contact with another, or with a stationary obstacle. In a biological context, collisions can be harmful (as when a prey is caught by a predator, or a pathogen passes from one animal to another), or beneficial (as when one ant exchanges chemical information with a nest mate, or a predator succeeds in capturing a prey).

© 2016 IOP Publishing Ltd

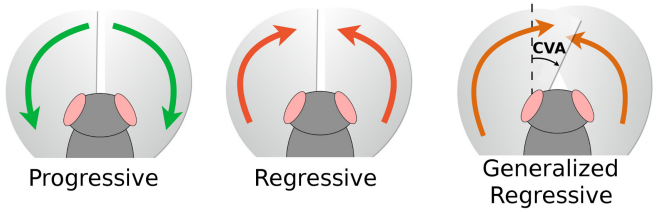

Figure 1. Progressive motion, regressive motion, and GRM. Progressive motion is any counter-clockwise motion perceived in the left visual hemifield and any clockwise motion perceived in the right visual hemifield. Regressive motion is any clockwise motion in the left visual hemifield and counter-clockwise motion in the right visual hemifield. GRM is motion towards the nasal boundary of either eye. Its perception depends on the azimuthal position of the nasal boundary of the visual field of each eye. We call the angular distance of the nasal visual boundary from the 0° (straight-ahead) azimuth the contralateral visual angle.

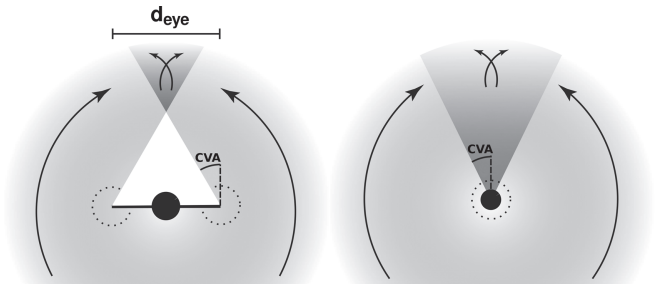

Figure 2. A geometric-point agent using GRM. Left: the arrows indicate directions of angular velocity on the agent's eyes that cause it to perceive GRM. d_{eye} indicates the agent's inter-eye distance. Right: if $d_{eye} = 0$ the two eyes coincide, but still detect GRM independently. As a result, any movement in a cone extending from the agent's eyes forward is GRM.

motion has not been explored by Zabala *et al* (2012). We build on the results of Zabala *et al* by providing a theoretical and practical analysis of generalized regressive motion (GRM)—visual stimulus similar to regressive motion but simpler to detect and more versatile. Whereas regressive motion occurs when there is clockwise motion in the left visual hemifield or counter-clockwise motion in the right visual hemifield, GRM occurs if there is clockwise motion in the left eye or counter-clockwise motion in the right eye, as shown in figure 1. Experiments by Zabala *et al* admit the hypothesis that the fruit fly uses GRM, not pure regressive motion, for stopping. We show that GRM enjoys the advantages of both looming motion and regressive motion. Our contribution is threefold:

- Whereas regressive motion alone is not a good cue to frontal collisions, we use geometric reasoning to show that GRM is a sufficient cue to prevent collisions whether both agents move, or one is a stationary obstacle.
- We argue that collisions ought not to be studied as an all-or nothing phenomenon. Rather the probability of avoiding collisions (here called 'safety') is a more informative parameter. We point out that avoiding unwarranted stops is an equally important performance criterion, which we call 'mobility'.
- With the help of agent-based modeling, we show that a population of Braitenberg-vehicle-like agents (Braitenberg 1986) using GRM as their sole collision-avoidance mechanism can be both safe from collisions and mobile when compared to looming-based agents.

Collision avoidance has been extensively studied in the fields of robotics and human locomotion. In the final section we discuss our work in that context in detail. We find that GRM-inspired algorithms require little computational power compared to existing methods. At the cost of allowing some unnecessary stops, GRM offers a low-power computational module for avoiding collisions between a mobile agent and mobile obstacles.

Geometry of regressive motion

Our geometric analysis of GRM is based on an abstract model of an agent: It is a point in the Euclidean plane, equipped with two 'eyes'—centers of projection. Each agent has a well-defined orientation, which allows us to define its contralateral visual angle (CVA). The CVA is the angle subtended by the nasal boundary of each eye, as in figure 1 (right). For now, we assume the distance between the eyes is zero and identify their position with the position of the agent (see figure 2). This assumption is justified if the modeled animal's inter-eye distance is small compared to its typical distance from other animals. We nevertheless drop this assumption in simulations (described below),

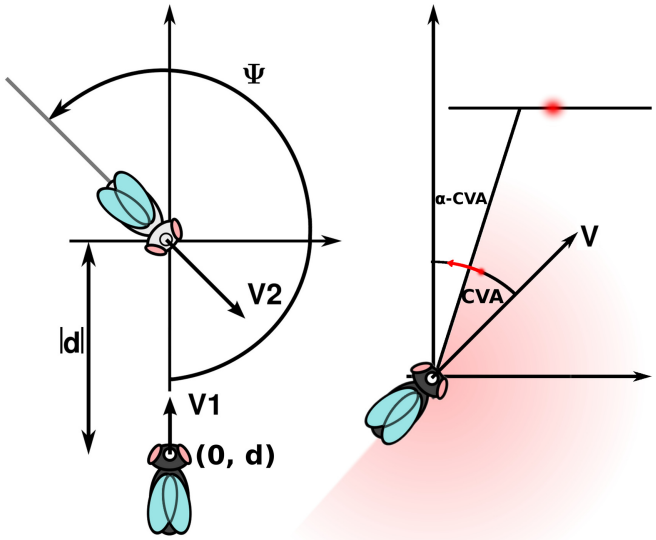

Figure 3. Reference frames for theorems 3 and 5. Left: when two agents—schematically shown as flies—have non-parallel velocities, we can describe every possible pair of trajectories using four parameters (see text). Right: when an agent with positive CVA approaches a flat wall sufficiently close, it can always observe GRM for some points on the wall (see text).

where we consider agents with two separate eyes and spatially extended bodies.

GRM detection can prevent all collisions among moving conspecifics

Let a point (which could be stationary or in movement) project to azimuthal position ϕ on the observer agent's eye. Let $\phi = 0$ be the direction in front of the agent, positive angles for the left side and negative angles for the right side, and restrict $\pi \in [-\pi, \pi)$. Denote the point's angular velocity as $\dot{\phi}$.

Definition 1. A point projecting at ϕ is in regressive motion with respect to the observer if $\dot{\phi} \cdot \phi \leqslant 0$, and in progressive motion otherwise.

Before proving our main theorem, we state an easy propsition whose proof we relegate to the mathematical appendix.

Proposition 2. *Let the relative position and velocity of the observed object be* x and v *respectively. Then* $\dot{\phi} = \frac{1}{\| \mathbf{x} \|^2} \langle \mathbf{v}^{\perp}, \mathbf{x} \rangle$. *In particular,* $\dot{\phi}$ *scales as one over distance squared.*

The following theorem ensures that before any potential collision, one of the agents will perceive regressive motion.

Theorem 3. *Let f1 and f2 be two agents moving on straight, intersecting trajectories. If f1 reaches the trajectory intersection after f2, f1 perceives regressive motion at all times before f2 reaches the intersection and progressive motion afterwards. f2 perceives progressive motion before f1 reaches the intersection, and regressive motion afterward.*

Proof. Let two point-agents f1, f2 move on a flat uniform surface with constant velocities on intersecting (that is, non-parallel) trajectories. Align the reference frame's y-axis with the direction of f1's movement, and place the origin at the point at which the agents' trajectories cross. The situation is fully described by four parameters (see figure 3 Left):

v^1, v^2—the speed of *f*1 and *f*2 respectively,

ψ—the angle *f*2's velocity vector makes with *f*1's velocity (also called the *angle of approach*), and

d—the y-coordinate of *f*1 at the moment when *f*2 reaches the origin.

First, we compute the angular position ϕ_{21} of *f*2 on *f*1's projection center and the angular velocity $\dot{\phi}_{21}$, at the moment when *f*1 is at distance $d + \epsilon$ from 0.

For $\epsilon = 0$, the positions of the two agents are respectively

$$x^1(d) = (0, d),$$
$$x^2(d) = (0, 0).$$

If $\epsilon \neq 0$, the time that passed since the original configuration is $\Delta t = \epsilon / v^1$, and since the velocity of *f*2 is $\mathbf{v}^2 = v^2(-\sin\Psi, \cos\Psi)$, we have

$$\mathbf{x}^1(d + \epsilon) = (0, d + \epsilon),$$
$$\mathbf{x}^2(d + \epsilon) = \epsilon \frac{v^2}{v^1}(-\sin\Psi, \cos\Psi).$$

Define $\mathbf{x}^R$, $\mathbf{v}^R$ to be the relative position and velocity of *f*2 in *f*1's frame of reference. Then

$$\begin{aligned}\mathbf{x}^{\mathrm{R}}(d+\epsilon) &= \mathbf{x}^2(d+\epsilon) - \mathbf{x}^1(d+\epsilon)\\ &= \left(-\frac{\epsilon v^2}{v^1}\sin\Psi,\ \frac{\epsilon v^2}{v^1}\cos\Psi - (d+\epsilon)\right),\\ \mathbf{v}^{\mathrm{R}}(d+\epsilon) &= (-v^2\sin\Psi,\ v^2\cos\Psi - v^1).\end{aligned}$$

From this we can directly compute ϕ_{21}, and proposition 2 enables us to compute the angular velocity of *f*2

$$\phi_{21} = \arctan(x_2^{\mathrm{R}}/x_1^{\mathrm{R}}) - \pi/2,$$
$$\dot{\phi}_{21} = \frac{1}{D^2}\langle \mathbf{v}^{\mathrm{R}\perp}, \mathbf{x}^{\mathrm{R}}\rangle,$$

where $D^2 = (x_1^{\mathrm{R}})^2 + (x_2^{\mathrm{R}})^2$ is the distance between the two agents. Plugging in the values calculated above we get

$$\phi_{21}(d,\epsilon) = \arctan\frac{\epsilon\frac{v^2}{v^1}\cos\Psi - (d+\epsilon)}{-\epsilon\frac{v^2}{v^1}\sin\Psi} - \pi/2, \tag{1}$$

$$\dot{\phi}_{21}(d,\epsilon) = -\frac{1}{D^2}dv^2\sin\Psi, \tag{2}$$

with $D^2 = \left(\frac{v^2\epsilon}{v^1}\right)^2 + (d+\epsilon)^2 - 2\epsilon\frac{v^2(d+\epsilon)}{v^1}\cos\Psi$.

Now, assume that *f*2 arrives at the intersection first, that is $d < 0$. From equation (2) it follows that

$$\dot{\phi}_{21}(d,\epsilon) \geqslant 0 \Leftrightarrow \sin\Psi \geqslant 0.$$

But this implies that the denominator in the arctangent in equation (1) is nonnegative if and only if $\epsilon \leqslant 0$

$$-\epsilon\frac{v_2}{v_1}\sin\Psi > 0 \Leftrightarrow \epsilon \leqslant 0,$$

A positive denominator restrict the range of the arctangent to $[-\pi/2, \pi/2]$, and thus

$$\epsilon \leqslant 0 \Leftrightarrow \phi \in [-\pi, 0].$$

Thus

$$\dot{\phi}_{21}(d,\epsilon) \geqslant 0 \Leftrightarrow (\phi(d,\epsilon) \in [-\pi, 0] \Leftrightarrow \epsilon \leqslant 0).$$

Analogously

$$\dot{\phi}_{21}(d,\epsilon) \leqslant 0 \Leftrightarrow (\phi(d,\epsilon) \in [0, \pi] \Leftrightarrow \epsilon \leqslant 0).$$

This proves the first part of the theorem. The second part is proven exactly in the same way, but switching the reference frame to that of *f*2. □

The theorem easily generalizes to GRM:

Definition 4. Let f2 project onto a projection center f1, with azimuthal position ϕ_{21}. f1 perceives GRM if and only if ($\dot{\phi}_{21} > 0$ and $\phi_{21} \in [-\pi, \mathrm{CVA}]$) or ($\dot{\phi}_{21} < 0$ and $\phi_{21} \in [-\mathrm{CVA}, \pi]$), where CVA is a fixed angle.

Theorem 5. *Let f1 and f2 be two agents moving on straight, intersecting trajectories. If f1 reaches the trajectory intersection after f2, f1 perceives GRM at all times before f2 reaches the intersection.*

This follows from theorem 3 because regressive motion implies GRM (see definitions above).

GRM detection can prevent collisions with stationary objects

An agent using solely non-GRM detection will always collide with stationary obstacles, which project expanding (progressive) patterns. However, GRM with CVA >0 and appropriate motion thresholding provides a mechanism for stationary collision avoidance. Let T_{GRM} denote the smallest magnitude of GRM that causes the agent to stop. Intuitively, larger CVA's and smaller T_{GRM} provide better obstacle detection.

Theorem 6. *An agent on a collision course with a stationary object will perceive GRM before the collision, as long as $T_{GRM} < \infty$ and CVA > 0.*

Proof. We assume the agent is approaching an object such that the centerline of the agent $\phi = 0$ does not point directly at a (non-smooth) corner of the object. We can then assume there is a neighborhood around the $\phi = 0$ aziumuth that can be approximated as a wall segment. As in figure 3 (right), place the origin at the position of the agent as shown. The agent approaches the wall at an angle $0 < \alpha < \pi/2$ and with positive speed v, its velocity $\mathbf{v} = (v\sin\alpha, v\cos\alpha)$. Consider an arbitrary wall-point (x, y), marked red in the figure. The relative velocity of the point w. r. t. the agent is $-\mathbf{v}$, and its angular velocity on the agent's eye equals (by proposition 2)

$$\dot{\phi}(x, y, \alpha, v) = \frac{-v}{x^2 + y^2}(x\cos\alpha - y\sin\alpha). \tag{3}$$

We need to take into account very small θ and very large T. The following proposition implies the theorem

$$\forall_{\theta, T>0}\ \exists_{X>0}\ \text{s.t.}\begin{cases}\|\dot{\phi}(X, y, \alpha, v)\| > T & \text{and}\\ y\tan(\alpha - \theta) > X > y\tan\alpha\end{cases},$$

where the last condition restricts the point we're searching for to be between the leftmost edge of perceived GRM and the center of the agent's visual field. Now, fix $X = y\tan\left(\frac{\alpha-\theta}{k}\right)$, $k > 1$. k can always be chosen to make the point (X, y) arbitrarily close to the centerline, and so contained in the smooth wall-like neighborhood on the obstacle. Clearly these X, y satisfy the second condition above. We also have

$$\dot{\phi}(X, y, \alpha, v) = \frac{-v\left(y\left[\tan\frac{\alpha-\theta}{k}\cos\alpha - \sin\alpha\right]\right)}{y^2\left(\tan\frac{\alpha-\theta}{k} + 1\right)}.$$

Since α, θ and k are constant, this expression scales as $1/y$ and thus reaches arbitrarily large magnitudes as y approaches 0—that is, as we place the observer closer and closer to the wall. □

The intuition behind this theorem is that a GRM detector detects any motion in a cone symmetrical about the center of the visual field. If the agent frontally approaches an object, the target is guaranteed to

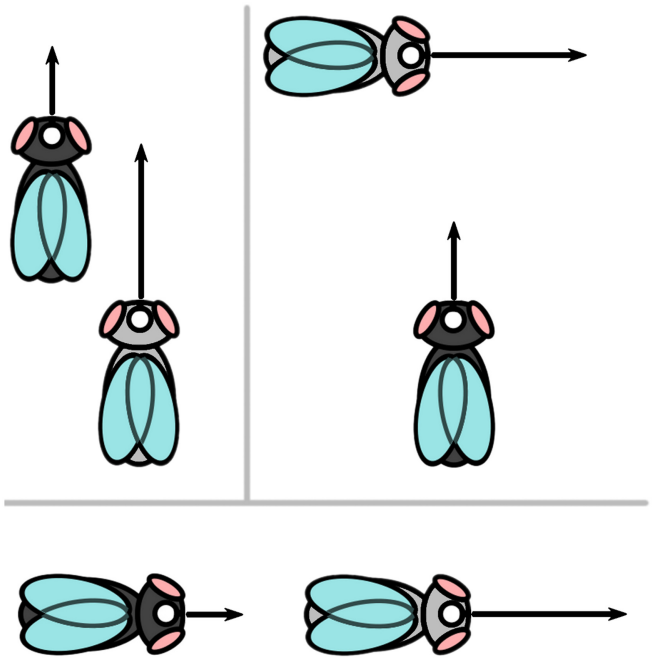

Figure 4. GRM false alarms arrow lengths indicate speeds. In each of the situations pictured collision is not imminent, but the darker agent perceives GRM. Left: the faster, bright agent takes over a slower one from behind. Right: the brighter agent crosses a trajectory junction in advance of the darker agent's arrival. Bottom: the faster, bright agent is moving away from the slower dark agent.

produce a strong enough signal within that cone at some positive time before the collision occurs.

False alarms, safety and mobility

Theorems 5 and 6 give basis to the claim that GRM can be useful for collision avoidance. However, it can be argued that they are of limited practical use. One problematic area not explored by the theorems is that of false alarms. An agent using GRM as a stopping cue can stop unnecessarily in a variety of situations, some of which are shown in figure 4.

If perception of GRM of any magnitude greater than zero caused the agents to stop, they would be perfectly safe from collisions, but unable to move. In simulations described below we investigate the role of two parameters that enable GRM-based agents to trade-off mobility and safety from collisions: the CVA and tne threshold T_{GRM} on the magnitude of GRM that stops the agent. Varying these parameters in a population of agents changes the population's safety and mobility, where safety corresponds to the fraction of prevented collisions, and mobility to the fraction of useful stops. Formally, we can classify any encounter between agents $f1$ and $f2$ as

True Positive (TP): agent $f1$ stops due to perceived motion of agent $f2$, and *$f1$ would collide with $f2$* had both $f1$ and $f2$ continued to move with velocities they had at the moment of $f1$'s stop, and $f2$ is outside of $f1$'s collision radius.

True Negative (TN): agent $f1$ moves without stopping and does not collide with any entity.

False Positive (FP): agent $f1$ stops due to perceived motion of entity $f2$, and *$f1$ would not collide with $f2$* had both $f1$ and $f2$ continued to move at velocities they had at the moment of $f1$'s stop. In addition, $f2$ is outside of $f1$'s collision radius at the time of stopping.

False Negative (FN): agent f1 collides with agent f2.

We can then define mobility and safety as

$$\text{mobility} = \frac{\text{TP}}{\text{TP} + \text{FP}} \text{ and}$$

$$\text{safety} = \frac{\text{TP}}{\text{TP} + \text{FN}}.$$

Mobility is high if and only if the agent rarely stops without a good reason. Safety is a complementary measure that is high if and only if the agent avoided many out of all the potential collisions. In our view, any collision avoidance algorithm is useful inasmuch as it offers a range of good mobility-safety tradeoffs: It can be used to make mobile vehicles remain relatively safe (relative to other algorithms), as well as safe vehicles that retain good mobility.

Simulations

A number of issues are not covered by our theory:

- real agents have extended bodies, unlike the geometric points considered in theorem 5,

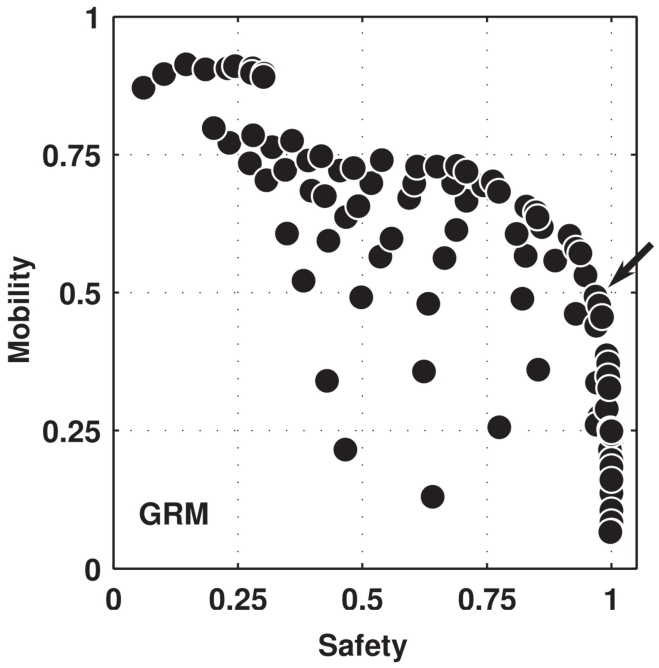

Figure 5. Mobility and safety of GRM-based collision avoidance. Each point corresponds to the mean mobility and safety achieved by GRM-based agents with fixed T_{GRM} and CVA (and T_{LOOM} set to a very large value, disabling looming-based collision avoidance in practice; see methods for more details). Each point corresponds to a different (T_{GRM}, CVA) value, used in 50 randomized repetitions of 50 s long simulations to estimate the means. A wide variety of safety-mobility tradeoffs are available, including a reasonable 50% mobility at 95% safety marked by the arrow.

- real agents have visual systems with multiple centers of projection and
- there is a tradeoff of safety and mobility to be explored.

Studying the tradeoff between mobility and safety is best done experimentally in a simulated environment. It is difficult to derive theoretical tradeoff curves given the statistical variability of the trajectories even in simple environments. Computational simulations are also a good tool for studying GRM agents with extended bodies and two separate eyes. Thus, to further study GRM we use agent-based modeling with populations of fly-like agents trying to avoid collisions. The agents use GRM- and looming-based algorithms for stopping. We compare the performance of GRM-based and looming-based collision avoidance using population safety and mobility as performance metrics. The details of the simulation setup are available in Methods below. Matlab code implementing the simulations is available online at http://vision.caltech.edu/~kchalupk/code.html.

GRM detection offers good mobility and safety to a population of conspecifics

In each simulation, ten fly-like agents were placed in a toroidal arena and followed straight trajectories with constant speed. Each agent was equipped with a stopping mechanism triggered by the perception of GRM with specific CVA and T_{GRM}(consistent across all the agents in a given simulation run). We performed 100 types of simulations, varying the CVA and T_{GRM} values systematically[5]. After running multiple trials for each simulation type, we calculated the safety and mobility of the agent population in each case. Figure 5 shows that varying the GRM parameters offers a wide variety of safety-mobility tradeoffs to the population.

Looming detection offers poor mobility and safety to a population of conspecifics

As a point of reference we measured the usefulness of looming as a signal for collision avoidance. To this goal, we equipped each agent with both a GRM and a looming detector. We then performed a series of simulations varying CVA, T_{GRM} and T_{LOOM}, where the latter is a looming threshold (methods contains a detailed description of the stopping mechanism). Figure 6 (left) shows safety and mobility in the simulations where only the looming signal was used for stopping (that is, T_{GRM} was very high). The figure shows that to achieve 95% safety, the agents had to stop unnecessarily 75% of the time. Figure 6 (middle, right) shows full simulation data: each marker corresponds to one (CVA, T_{GRM}, T_{LOOM}) setting, and the three parameters vary independently. In figure 6 (middle) the value of T_{GRM} varies smoothly on the upper envelope of

[5] The agents were also equipped with a looming detector, which in the simulations described in this section was set to be extremely insensitve.

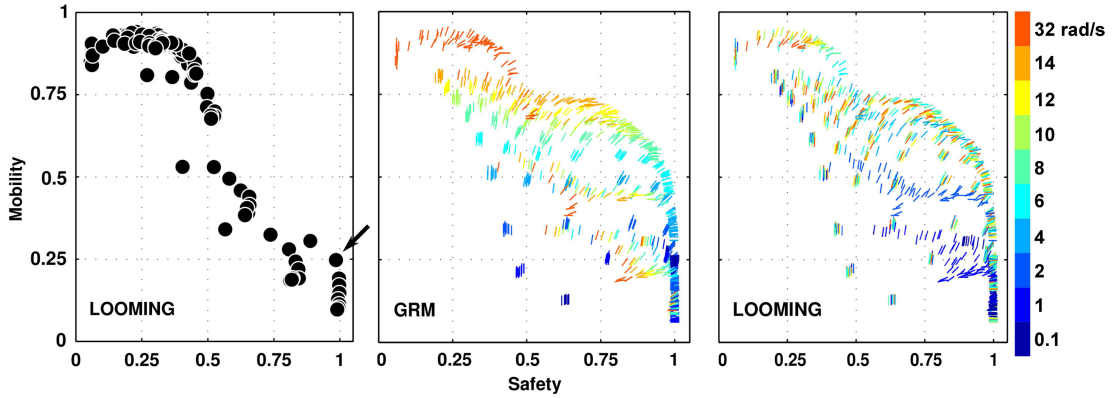

Figure 6. Mobility and safety of GRM- and looming-based collision avoidance. Each point corresponds to a different (T_{GRM}, T_{LOOM}, CVA) value, used in 50 randomized repetitions of 50 s long simulations to estimate the means. Its position is at the mean safety and mobility of a population of agents over the 50 trials. Left: only points with $T_{GRM} = 32$ rad s^{-1} (that is, GRM detection practically disabled) are shown. The arrow points to the highest-mobility point with more than 95% safety. Middle: points for all the possible (T_{GRM}, T_{LOOM}, CVA) settings. The angle of each bar is the CVA used in corresponding simulations, while the bar's color equals T_{GRM}. Right: as Middle, but the colors now correspond to T_{LOOM}. For example, the leftmost top point corresponds to CVA = 0, $T_{GRM} = 32$, $T_{LOOM} = 4$. This point has high mobility and low safety. This is because its low CVA and high T_{GRM} can not prevent many collisions; at the same time, relatively low T_{LOOM} does not seem to help much with collision avoidance.

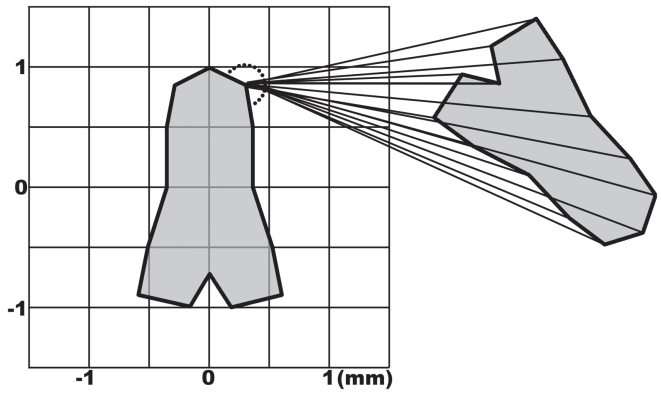

Figure 7. Outline of a simulated fly agent. Each agent in our simulations is defined by 14 points, as shown in the figure. The agent's two eyes (only the right eye is shown) compute at each time step the angular projections and velocities of the 14 defining points of each other visible agent.

the scatter plot. It is very clear that choosing low T_{GRM} offers good safety but bad mobility, whereas higher T_{GRM} increases safety but decreases mobility. Figure 6 (right) shows that the correspondence between T_{LOOM} and the safety-mobility tradeoff is much less clear. Whereas low values of T_{LOOM} decrease mobility of the agents, increasing the value past a certain point offers no additional safety-mobility advantages when GRM is also used for collision avoidance.

Methods: simulation parameters

Each simulation puts ten fly-like agents, each defined by 14 visible points (see figure 7), in a toroidal arena—a square of side length 50 mm with opposing edges glued together.

The flies follow simple dynamics, described below. For each combination of CVA $\in \{0, 10, \ldots, 90\}$ degrees and T_{GRM}, $T_{LOOM} \in \{0.1, 1, 2, 4, 6, 8, 10, 12, 14, 32\}$ rad s^{-1}, we ran 50 trials of 10 000 time-steps (to a total of 1000×50 simulations, 50 s long each, of flies walking at realistic speeds). Movies S1-S4, available online at http://vision.caltech.edu/~kchalupk/code.html, show four example simulation runs resulting from different parameter settings. (Movie captions appendix describes symbols used in the movies.)

Numerical implementation: the motion and control of each agent are computed at discrete time-intervals with constant time increments of Δt. For simplicity of notation where we write $t + 1$ in the following, we mean $t + \Delta t$. The value of Δt is given in table 1 alongside all other simulation parameters.

Agent trajectories: the ith agent's trajectory is determined by walking speed v_i, initial position $\vec{x}_i^0$ and

Table 1. Parameters defining the fly model.

Symbol	Default value	Meaning
Δt	0.005 s	Time-step in numerical simulations
R	50 mm	Edge length of the walking arena (glued into a torus)
N	10	Number of flies in the arena
l	2 mm	Length of an agent
d	0.55 mm	distance between the eyes' centers
$v_{\min}$	10 mm s^{-1}	minimum agent speed
$v_{\max}$	30 mm s^{-1}	maximum agent speed
v_i	$\sim U(v_{\min}, v_{\max})$	walking velocity of agent i
p_{01}	~0.8	prob. stop-to-walk in a 1 s time-interval
P_{01}	0.008	prob. stop-to-walk in one time-interval (i.e. $(1-p_{01})^{\Delta t} = (1-P_{01})$)
T_{LOOM}	0° s^{-1} (†)	stopping threshold on looming motion
T_{GRM}	0° s^{-1} (†)	stopping threshold on regressive motion
CVA	30° (†)	the CVA
θ_i	120°	angle of ipsilateral visual field seen by each eye
δ_σ	30°	increment of standard deviation of agent reorientation motions $\sigma_{\vec{v}}$
λ_σ	0.992	decay constant for $\sigma_{\vec{v}}$ at each Δt
n	14	number of points on each agent
	(†)	variable whose value is systematically explored in some experiments

initial direction $\vec{v}_i$ with $\|\vec{v}_i\| = 1$, i.e. $\vec{x}_i(t) = \vec{x}_i^0 + tv_i\vec{v}_i$. Each agent has a different constant velocity chosen uniformly from the [1–3] cm s^{-1} interval.

Control: while it is walking, each agent keeps walking at constant velocity until it is stopped by a GRM or looming percept caused by another agent (as explained below).

Spontaneous start: when an agent is stationary it flips a coin at each time step: if the coin turns out to be heads, the agent starts moving in the current direction at its preferred velocity. If the coin is tails it stays put. The probability of obtaining heads in the interval of 1 s is denoted p_{01}; thus, the probability of obtaining tails in one time-step is $(1-p_{01})^{\Delta t}$.

Orientation: while an agent is walking, it keeps constant velocity and orientation (i.e. $\vec{v}_i(t+1) = \vec{v}_i(t)$). Upon stopping it samples a new orientation from a Gaussian pdf with standard deviation equal to the current value of a parameter σ_i and centered at the current orientation. In addition, after reorientation, σ_i increases by a fixed amount δ_σ. σ_i decays exponentially, with decay constant λ_σ, i.e. $\sigma_i(t + k\Delta t) = \sigma_i(t)\lambda_\sigma^k$. This mechanism, modeling basic neuronal sensitization, is a simple way to allow the flies to keep roughly straight trajectories when encountering transient obstacles (other moving flies), and avoid getting stuck around large static obstacles (groups of stopped flies).

GRM: each eye sees GRM whenever the angular motion of any point projecting onto its retina is directed contralaterally, i.e. counterclockwise for the right eye and clockwise for the left eye. Each eye's visual field goes beyond the frontal direction to cover a given CVA. The CVA is a free parameter which we study to discover the best compromise between avoiding collisions and false alarms.

GRM stops: agent boundaries are defined by 14 points visible to other flies, as shown in figure 7. Call the jth point on the ith agent p_j^i and its azimuthal position on the observer's eye $\phi(p_j^i)$. Each agent measures the angular velocity of all the points on the other flies. If *any* GRM $\dot{\phi}(p_j^i)$ is detected, the agent compares the GRM magnitude $\|\dot{\phi}(p_j^i)\|$ to a threshold T_{GRM} and stops if $\|\dot{\phi}(p_j^i)\| > T_{\mathrm{GRM}}$.

Looming motion: Let $\|\dot{\phi}_{\mathrm{L}}\|$ denote the largest magnitude of counter-clockwise motion that any point evokes in the left visual hemifield, and $\|\dot{\phi}_{\mathrm{R}}\|$ the largest magnitude of clockwise motion evoked in the right visual hemifield. Then the strength of looming perceived by the agent equals $\omega_{\mathrm{LOOM}} := \min(\|\dot{\phi}_{\mathrm{L}}\|, \|\dot{\phi}_{\mathrm{R}}\|)$.

Looming stops: similarly to GRM stopping, the agent stops if $\omega_{\mathrm{LOOM}} > T_{\mathrm{LOOM}}$. This simple mechanism activates only if the agent can perceive points diverging at velocities larger than T_{LOOM}.

All simulation parameter values are specified in table 1. To summarize, agent i's motion is governed by the following equations (see also the diagram in figure 8).

In order to simplify the notation we omit index i unless necessary, and write out the equations for a one-eyed agent; since both looming and GRM are monocular cues in our implementation, the extension to the two-eyed agent is trivial.

Control: Let $z \in \{0, 1\}$ be the variable denoting whether an agent is stationary ($z = 0$) or in motion

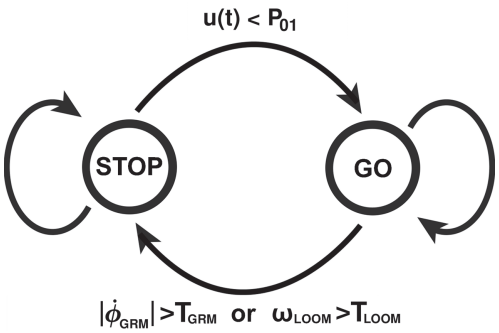

Figure 8. Simulated agents, a control diagram. Each fly-like agent keeps following a straight trajectory (see text for details) until either regressive motion or looming expansion on its retina exceeds a fixed threshold. The agent then stops until a Bernoulli coin (tossed on each time step) shows 'heads'.

($z = 1$). Let $u(t)$ be an i.i.d. random process with uniform probability density on $(0, 1)$. Let $\|\dot{\phi}_{\mathrm{GRM}}(t)\|$ be the largest observed magnitude of GRM at time t. Let $\omega_{\mathrm{LOOM}}(t) := \min(\|\dot{\phi}_{\mathrm{L}}(t)\|, \|\dot{\phi}_{\mathrm{R}}(t)\|)$ denote the looming strength observed at time t.

$$z(0) = 1 \quad \text{initially the agent is set in motion}$$

$$z(t+1) = \begin{cases} 0 & \text{if } z(t) = 1 \text{ and} \\ & (\|\dot{\phi}_{\mathrm{GRM}}(t)\| > T_{\mathrm{GRM}} \text{ or} \\ & \omega_{\mathrm{LOOM}}(t) > T_{\mathrm{LOOM}}) \\ 1 & \text{if } z(t) = 0 \text{ and} \\ & \|\dot{\phi}_{\mathrm{GRM}}(t)\| < T_{\mathrm{GRM}} \text{ and} \\ & \omega_{\mathrm{LOOM}}(t) < T_{\mathrm{LOOM}} \text{ and} \\ & u(t) < P_{01} \\ z(t) & \text{otherwise.} \end{cases}$$

Trajectory: Call $\vec{v}$ the direction vector, i.e. $\|\vec{v}\| = 1$. With a slight abuse of notation use $\vec{v}$ also for the angle of $\vec{v}$, i.e. write $\vec{v} \sim G(\cdot; \mu, \sigma)$ to indicate that the angle of $\vec{v}$ is drawn from a given Gaussian density mod 2π[6].

$$\begin{aligned} x(0) &\sim U(A) \\ v(0) &\sim U(v_{\min}, v_{\max}) \\ \vec{v}(0) &\sim U(0, 2\pi) \\ x(t+1) &= x(t) + v(t)\vec{v}(t)\Delta t \\ v(t+1) &= z(t)v \\ \vec{v}(t+1) &\sim \begin{cases} G(\cdot; \vec{v}(t), \sigma_{\vec{v}}(t)) \\ \quad \text{if } z(t) - z(t+1) = 1 \\ \vec{v}(t) \text{otherwise.} \end{cases} \end{aligned}$$

Direction change standard deviation:

$$\begin{aligned} &\sigma_{\vec{v}}(0) = 0, \\ &\sigma_{\vec{v}}(t+1) = \lambda_\sigma \sigma_{\vec{v}}(t) + \delta_\sigma(1 - z(t))z(t-1). \end{aligned}$$

[6] A is the surface of the walking arena. We re-draw the initial positions so that the flies do not overlap at $t = 0$.

Discussion

Our results show that GRM constitutes a good cue for collision avoidance. Extending the analysis of Zabala *et al* (2012), we showed both mathematically and in simulations that increasing the CVA to a non-zero value improves collision avoidance. In particular, it allows the detection of both stationary and moving objects on a collision course. In this respect, GRM can be viewed as a computationally efficient way to connect looming detection with regressive motion detection. We introduced safety and mobility as collision avoidance performance metrics and used looming as a reference point to show that GRM is a better cue for collision avoidance among conspecifics.

Relevance to robotics and human locomotion

Multi-agent navigation has been studied extensively in robot and human locomotion. It is of practical importance in applications involving robotic assembly, demining and search and rescue missions, as well as understanding of crowd behavior and preventing crowd disasters.

Two main problems arise in multi-agent navigation: finding the way to the goal and avoiding collisions while approaching it. Our work only attempts to solve the second problem. Nevertheless, it is easy to envision GRM-based navigation, for example following the general approach of Van den Berg *et al* (2008): each agent chooses a heading that is as close as possible to the target heading, but does not elicit GRM on its retina. The most striking difference between this approach and extant work is that GRM requires very little computation, from cues directly accessible from the retinal projections and the optical flow.

Cutting *et al* (1995) analyze what information a mobile observer with mobile, fixating eyes requires for navigation. The fruit fly has immobile, non-fixating eyes. Despite this difference, our basic finding agrees with Cutting's seminal work: in a mobile world the gaze-movement angle, not looming, provides crucial information as to whether a collision will occur. It is interesting to note that Cutting arrives at this result by a careful experimental analysis of human perception, while we arrived at it analyzing a simplified model of fruitfly behavior.

Inspired by Cutting, Ondřej *et al* (2010) develop a simple principle for collision avoidance in crowded scenes: redirect if (1) the bearing of the obstacle is constant and (2) the time until the observer reaches the closest point to the obstacle is positive. However, even the simple task of detecting whether the bearing angle of a specific object is constant requires segmentation of the scene, because an object's projection expands and contracts as the it approaches and departs. In addition, Ondřej *et al*'s algorithm requires the observer to know (or infer from angular expansion rates,

which presupposes segmentation) the positions and velocities of all obstacles.

An alternative to biologically-inspired approaches is to construct a mathematical model of navigation from first principles. Fajen *et al* (2003) derive an elegant dynamical model for multi-agent navigation and set its parameters using human behavior data. However, the model assumes each agent's knowledge of distances to all obstacles. Huang *et al* (2006) adapt the algorithm for use with single-camera robots by substituting that information with a function of the width of the obstacle on the retina. This, however, requires at least coarse scene segmentation. Similarly, any algorithm that depends on time-to-collision estimates (Karamouzas *et al* 2014) relies on successful scene segmentation.

Van den Berg *et al* (2008) (and later Van den Berg *et al* (2011)) study *reciprocal collision avoidance*: similar to us, they assume that the agents all implement the same movement protocol. However, they also assume that each agent knows the positions, velocities, and exact shapes of all other agents.

Whereas scene segmentation and obstacle positions and velocities can be computed with modern mechanical sensors, we showed that collision avoidance is possible with even simpler cues. GRM is biologically feasible and can be computed using Reichardt-detector-like circuits (Reichardt 1961). Such circuits have been successfully implemented on minimalistic hardware (Barrows *et al* 2002, Beyeler *et al* 2009).

GRM-based control is thus at the lower end of the spectrum of navigation algorithms ordered by the complexity of the cues they rely on. The algorithms discussed in this section trade simplicity for better and more natural-looking navigation. Yet more sophisticated algorithms for robotic navigation, e.g. Probabilistic Roadmaps (Kavraki *et al* 1996, Boor *et al* 1999, Karaman and Frazzoli 2011) or Rapidly Exploring Random Trees (LaValle 1998, Petti and Fraichard 2005, Kuwata *et al* 2009, Karaman and Frazzoli 2011), require significantly larger computational power. Importance of low-complexity collision avoidance grows as fields such as drone flight control are rapidly developing (Pines and Bohorquez 2006, Kushleyev *et al* 2013, Lentink 2014, Virágh *et al* 2014).

GRM and biology

Whereas perception of regressive motion appears to influence the behavior of the fruit fly, the neural circuitry participating in this perception-action loop remains unknown. Fotowat and Fayyazuddin (2009) and de Vries and Clandinin (2012) showed that looming-sensitive neurons in *Drosophila* participate in a neural pathway that mediates escape behavior. However, escape is not the same as collision avoidance. We showed that looming might not be a practical collision-avoiding solution for groups of interacting animals as it can overly impede the mobility of a group. We argue that further research into the neural circuitry of GRM-based action in animals is an important future direction.

One reason why regressive motion has remained a relatively obscure phenomenon might be the often overlooked difference between static and dynamic environments when testing collision avoidance algorithms. For example, Blanchard *et al* (2000) constructed a robot guided by responses mimicking those of the locust looming-detection neurons. However, the robot's collision avoidance was only tested in an environment consisting of stationary obstacles. We have shown that in a more interactive environment, GRM has significant advantages over looming.

Acknowledgments

We thank the anonymous reviewers for excellent pointers to relevant literature. This work was supported by National Science Foundation grants 0914783 and 1216045, NASA Stennis grant NAS7.03001 and ONR MURI grant N00014-10-1-0933.

Mathematical appendix

Proposition 2. *Let the relative position and velocity of the observed object be* $\mathbf{x}$ and $\mathbf{v}$ *respectively. Then* $\dot{\phi} = \frac{1}{\|\mathbf{x}\|^2}\langle \mathbf{v}^{\perp}, \mathbf{x}\rangle$. *In particular, angular velocity scales as one over distance squared.*

Proof. We wish to derive the angular velocity of a point in relative motion projecting onto an observer. Place the center of projection at the origin, and a particle moving with constant velocity $\mathbf{v} = (u, v)$ at position $\mathbf{x}_0 = (x_0, y_0)$ at time 0, as shown in figure 9.

The position at time t equals $\mathbf{x} = \mathbf{x}_0 + t\mathbf{v}$, and the azimuth of the particle ϕ is such that

$$\tan\phi = \frac{\mathbf{y}}{\mathbf{x}} = \frac{y_0 + vt}{x_0 + ut}.$$

Taking the time derivative on both sides gives

$$\frac{1}{\cos^2\phi}\dot{\phi} = \frac{v(x_0 + tu) - u(y_0 + tv)}{(x_0 + ut)^2}$$

and thus

$$\dot{\phi} = \frac{\cos^2\phi\,(v(x_0 + tu) - u(y_0 + tv))}{(x_0 + tu)^2} \tag{4}$$

$$= \frac{(x_0 + tu)^2(v(x_0 + tu) - u(y_0 + tv))}{D^2(x_0 + tu)^2}, \tag{5}$$

where D is the distance of the particle from the origin. Equation (5) follows from the relation $\cos\phi = \frac{x_0 + tu}{D}$ (see figure 9). Simplifying the RHS yields

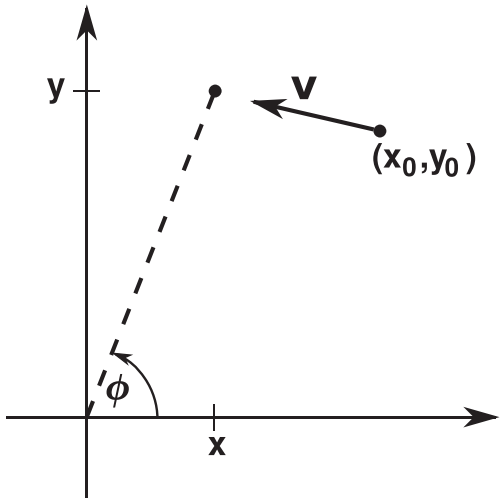

Figure 9. Calculating angular velocity. A particle moving with velocity $\mathbf{v}$ projects angular velocity $\dot{\phi}$ on the origin.

$$\dot{\phi} = \frac{v(x_0 + tu) - u(y_0 + tv)}{D^2} \tag{6}$$

$$= \frac{1}{\|\mathbf{x}\|^2}\langle \mathbf{v}^{\perp}, \mathbf{x}\rangle. \tag{7}$$

Since the position $\mathbf{x}$ moves on a line perpendicular to $\mathbf{v}^{\perp}$ we expect the dot product to be constant, and indeed it equals $vx_0 - uy_0$. Hence angular velocity decays as one over distance squared. □

Movie captions appendix

Available online are supplementary movies S1–S4. The movies show full trials of our simulations for chosen parameter settings. In each movie, ten fly-like vehicles are visible, colored arbitrarily to make tracking the vehicles easy. Whenever two vehicles collide, their body size is temporarily increased. Whenever a vehicle stops, it is surrounded by a colored circle. A red circle means the stop is a False Positive. A green circle indicates a True Positive. In addition, a line segment is drawn from the stopping vehicle to the one (or more) causes of its stop.

Movie S1: CVA $= 10°$, $T_{\mathrm{GRM}} = 6\,\mathrm{rad\,s^{-1}}$, $T_{\mathrm{LOOM}} = 32\,\mathrm{rad\,s^{-1}}$. In this movie, GRM is the stopping mechanism, and the CVA is small. An interesting situation arises at about 00:10, where three vehicles (bright green, blue, and yellow) meet. Green stops due to blue's motion, but unnecessarily. Blue avoids a collision with yellow. Yellow in turn crashes into green. That is because green is already stationary, so the GRM magnitude it evokes on yellow's retina is relatively small, and the small CVA prevents yellow from picking up any strong signals from stationary obstacles.

Movie S2: CVA $= 70°$, $T_{\mathrm{GRM}} = 6\,\mathrm{rad\,s^{-1}}$, $T_{\mathrm{LOOM}} = 32\,\mathrm{rad\,s^{-1}}$. This time, the CVA is large. This makes it easy for the flies to detect stationary obstacles on time. There are few collisions, but many unnecessary stops. The collision at 00:22 (blue and bright-green) is a good example of the type of collision that is hard to avoid using GRM detection. The vehicles' relative motion is insignificant, making the evoked GRM signal small.

Movie S3: CVA $= 10°$, $T_{\mathrm{GRM}} = 32\,\mathrm{rad\,s^{-1}}$, $T_{\mathrm{LOOM}} = 6\,\mathrm{rad\,s^{-1}}$. In this case the CVA is small and looming is the significant stopping mechanism. Collisions with stationary obstacles are hard to detect, mainly because the CVA is rather small (for example, three of them happen roughly at the same time at 00:04).

Movie S4: CVA $= 70°$, $T_{\mathrm{GRM}} = 32\,\mathrm{rad\,s^{-1}}$, $T_{\mathrm{LOOM}} = 6\,\mathrm{rad\,s^{-1}}$. Looming with large CVA. Encounters such as the light-blue fly stopping at 00:15 emphasize that simple looming mechanism (such as the one used in our simulation) do not know about figure-ground segmentation. The two flies that caused the stop are perceived as one expanding entity on light-blue's eye.

References

Barrows G L, Chahl J S and Srinivasan M V 2002 Biomimetic Visual Sensing and Flight Control Seventeenth *International Unmanned Air Vehicle Systems Conference* (pp. 1–15). Unmanned Air Vehicle Systems Association (UAVS)

Beyeler A, Zufferey J C and Floreano D 2009 Vision-based control of near-obstacle flight *Auton. Robots* **27** 201–19

Blanchard M, Rind F C and Verschure P F M J 2000 Collision avoidance using a model of the locust LGMD neuron *Robot. Auton. Syst.* **30** 17–38

Boor V, Overmars M H and van der Stappen A F 1999 The Gaussian sampling strategy for probabilistic roadmap planners *IEEE Int. Conf. on Robotics and Automation* pp 1018–23

Braitenberg V 1986 *Vehicles: Experiments in Synthetic Psychology* (Cambridge, MA: MIT Press)

Cutting J E, Vishton P M and Braren P A 1995 How we avoid collisions with stationary and moving objects *Psychol. Rev.* **102** 627

de Vries S E J and Clandinin T R 2012 Loom-sensitive neurons link computation to action in the drosophila visual system *Curr. Biol.* **22** 353–62

Eichner H, Joesch M, Schnell B, Reiff D F and Borst A 2011 Internal structure of the fly elementary motion detector *Neuron* **70** 1155–64

Fajen B R, Warren W H, Temizer S and Kaelbling L P 2003 A dynamical model of visually-guided steering, obstacle avoidance, and route selection *Int. J. Comput. Vis.* **54** 13–34

Fotowat H and Fayyazuddin A 2009 A novel neuronal pathway for visually guided escape in Drosophila melanogaster *J. Neurophysiol.* **102** 875–85

Gabbiani F, Krapp H G, Koch C and Laurent G 2002 Multiplicative computation in a visual neuron sensitive to looming *Nature* **420** 320–4

Hatsopoulos N, Gabbiani F and Laurent G 1995 Elementary computation of object approach by wide-field visual *Neuron Sci.* **270** 1000–3

Huang W H, Fajen B R, Fink J R and Warren W H 2006 Visual navigation and obstacle avoidance using a steering potential function *Robot. Auton. Syst.* **54** 288–99

Karaman S and Frazzoli E 2011 Sampling-based algorithms for optimal motion planning *Int. J. Robot. Res.* **30** 846–94
Karamouzas I, Skinner B and Guy S J 2014 Universal power law governing pedestrian interactions *Phys. Rev. Lett.* **113** 238701
Kavraki L E, Svestka P, Latombe J C and Overmars M H 1996 Probabilistic roadmaps for path planning in high-dimensional configuration spaces *IEEE Trans. Robot. Autom.* **12** 566–80
Kushleyev A, Mellinger D, Powers C and Kumar V 2013 Towards a swarm of agile micro quadrotors *Auton. Robots* **35** 287–300
Kuwata Y, Karaman S, Teo J, Frazzoli E, How J P and Fiore G 2009 Real-time motion planning with applications to autonomous urban driving *IEEE Trans. Control Syst. Technol.* **17** 1105–18
LaValle S M 1998 Rapidly-exploring random trees: a new tool for path planning
Lee D N and Reddish P E 1981 Plummeting gannets: a paradigm of ecological optics *Nature* **293** 293–4
Lentink D 2014 Bioinspired flight control *Bioinspiration Biomimetics* **9**
Ondřej J, Pettré J, Olivier A-H and Donikian S 2010 A synthetic-vision based steering approach for crowd simulation *ACM Trans. Graph.* **29** 123
Petti S and Fraichard T 2005 Safe motion planning in dynamic environments *IEEE/RSJ International Conference on Intelligent Robots and Systems* 2210–5
Pines D and Bohorquez F 2006 Challenges facing future Micro-Air-Vehicle development *J. Aircr.* **43** 290–305
Preuss T, Osei-Bonsu P E, Weiss S A, Wang C and Faber D S 2006 Neural representation of object approach in a decision-making motor circuit *J. Neurosci.* **26** 3454–64
Reichardt W 1961 Autocorrelation, a principle for the evaluation of sensory information by the central nervous system *Sensory Communication* ed W A Rosenblith (Cambridge MA: MIT Press) pp 303–17
Rind F C and Simmons P J 1992 Orthopteran DCMD neuron: a reevaluation of responses to moving objects: I. Selective responses to approaching objects *J. Neurophysiol.* **68** 1654–66
Schiff W, Caviness J A and Gibson J J 1962 Persistent fear responses in rhesus monkeys to the optical stimulus of 'looming' *Science* **136** 982–3
Sun H and Frost B J 1998 Computation of different optical variables of looming objects in pigeon nucleus rotundus neurons *Nat. Neurosci.* **1** 296–303
Takemura S Y *et al* 2013 A visual motion detection circuit suggested by Drosophila connectomics *Nature* **500** 175–81
Van den Berg J, Guy S J, Lin M and Manocha D 2011 Reciprocal n-body collision avoidance *Robotics Research* (Berlin: Springer) pp 3–19
Van den Berg J, Lin M and Manocha D 2008 Reciprocal velocity obstacles for real-time multi-agent navigation *IEEE Int. Conf. on Robotics and Automation (ICRA) 2008* pp 1928–35
Virágh C, Vásárhelyi G, Tarcai N, Szörényi T, Somorjai G, Nepusz T and Vicsek T 2014 Flocking algorithm for autonomous flying robots *Bioinspiration Biomimetics* **9**
Wang Y and Frost B J 1992 Time to collision is signalled by neurons in the nucleus rotundus of pigeons *Nature* **356** 236–8
Zabala F, Polidoro P, Robie A and Branson K 2012 A simple strategy for detecting moving objects during locomotion revealed by animal-robot interactions *Curr. Biol.* **22** 1344–50